Journal of Advanced Ceramics
2017, **6**(2): 120–128
DOI: 10.1007/s40145-017-0224-6

ISSN 2226-4108
CN 10-1154/TQ

Research Article

Effect of texture microstructure on tribological properties of tailored Ti_3AlC_2 ceramic

Ludi XU[a], Degui ZHU[a], Salvatore GRASSO[b], Tohru S. SUZUKI[c], Akira KASAHARA[c], Masahiro TOSA[c], Byung-nam KIM[c], Yoshio SAKKA[c], Minhao ZHU[a], Chunfeng HU[a,*]

[a]*Key Laboratory of Advanced Technologies of Materials*, *Ministry of Education*, *School of Materials Science and Engineering*, *Southwest Jiaotong University*, *Chengdu 610031*, *China*
[b]*School of Engineering and Material Science*, *Queen Mary University of London*, *London E1 4NS*, *UK*
[c]*National Institute for Materials Science*, *Tsukuba*, *Ibaraki 305-0047*, *Japan*

Received: January 08, 2017; Revised: March 14, 2017; Accepted: March 17, 2017

Abstract: Tribological property of *c*-axis textured shell-like Ti_3AlC_2 ceramic was investigated using reciprocating sliding balls (SUS304) under loads of 1, 5, and 9 N. It was found that the textured top surface (TTS), corresponding to the (000*l*) plane, shows the lowest mean coefficient of friction in comparison with those measured on the textured side surface (TSS), where the sliding directions are parallel (TSS-1) and perpendicular (TSS-2) to *c* axis, under the same load. Among all the tested orientations, the TSS-2 exhibited the lowest wear rate of 1.51×10^{-3} $mm^3/(N\cdot m)$ under the load of 9 N. The worn mechanisms on the TTS and TSS-1 were delamination, grain fracture, and grain spalling-off. On the TSS-2, plowing effect against balls was the dominating mechanism. This work suggests the criteria to maximize the wear resistance in the load range of 1–9 N.

Keywords: tailored Ti_3AlC_2; mean coefficient of friction; wear rate; worn mechanisms

1 Introduction

Ternary compounds $M_{n+1}AX_n$ phases (M is the transition metal, A is the A group element, X is C or N, and generally $n = 1–3$) belong to a large family with nanolaminar microstructure and hexagonal crystal structure (space group *P*63/*mmc*) [1–5]. To date, more than fifty 211 phases, five 312 phases, and eight 413 phases (excluding solid solutions) have been discovered. Recently, it has been confirmed that 514, 615, and 716 phases also exist [6–8]. Therefore, *n* values could be extended to 4, 5, and 6. Interestingly, a new nanolayered 221 phase, Mo_2Ga_2C, has been recently synthesized by solid/liquid reaction and magnetron sputtering [9]. It is a new type of MAX phase not belonging to the formula $M_{n+1}AX_n$, and more 221 phases might be discovered in the following years.

Since 1996, it has been demonstrated that some of MAX phases, such as Ti_3SiC_2, Ti_3AlC_2, Ti_2AlC, Cr_2AlC, etc., possess an unique combination of high Young's modulus, high flexural strength, high fracture toughness, excellent thermal shock resistance, and oxidation resistance [10–13]. Notably, it was found that these phases offer an excellent corrosion resistance against molten Pb above 850 ℃ together with good irradiation resistance to neutron and Kr, Xe, Au ions [14–16]. Therefore, they could be good candidates for

* Corresponding author.
E-mail: chfhu@live.cn

use in the fourth generation nuclear plants.

As for advanced structural materials, tribological properties of MAX phases are very important. Gupta *et al*. [17] systemically investigated the tribological behaviors of Ti_2AlC, Cr_2AlC, Ta_2AlC, Ti_3SiC_2, Ti_2AlN, Ti_4AlN_3, Cr_2GeC, Cr_2GaC, Nb_2SnC, and Ti_2SnC, tested against Ni-based superalloys at ambient and high temperatures (550 ℃). It was determined that at room temperature the wear rates are relatively high ($\geqslant 10^{-4}$ mm^3/(N·m)) due to abrasion against the third body. At 550 ℃, oxidized transfer films formed on both contacting surfaces, and their lubricant function contributed to a reduced wear rate ($< 10^{-6}$mm^3/(N·m)) [17]. Also, they found that if the counterpart is alumina against Ta_2AlC, Ti_2AlC, Cr_2AlC, and Ti_3SiC_2, even when tested under dry sliding conditions at 550 ℃, no visible wear track is observed and tribofilms are mainly constituted of amorphous oxides of M and A elements [18].

In wet and aggressive conditions (hydrochloric acid, alkalis, water, and ethanol), the tribo-corrosion behaviors of Ti_3SiC_2/Si_3N_4 countercouple were investigated. Even if the formation of SiO_2 film decreased the coefficient of friction (COF), this was not effective to prevent grains detaching from the bulk. In Ti_3SiC_2, mechanical damage dominated the wear behavior rather than the chemical corrosion [19,20].

Zhu *et al.* [21] systematically investigated the dry sliding tribological behaviors of Ti_3SiC_2 at room temperature in air, coupled with different counterfaces, including Ti_3SiC_2, Al_2O_3, Si_3N_4, SiC, and GCr15-bearing-steel. The highest wear rate (1.87×10^{-3} mm^3/(N·m)) was observed in the Ti_3SiC_2/Ti_3SiC_2 friction pair. However, the lowest wear rate (2.09×10^{-4} mm^3/(N·m)) was obtained in the Ti_3SiC_2/SiC friction pair. They found that oxide films protect the surface of Ti_3SiC_2/SiC friction pair from direct contact and decrease wear rate [21].

In order to enhance the wear resistance, Wan *et al*. [22] fabricated the SiC reinforced $Ti_3Si(Al)C_2$ composites (10–30 vol%) and tested against AISI-52100 steel balls at room temperature. They found that with increasing SiC content, both the coefficient of friction and wear rate are significantly decreased. The enhanced wear resistance was mainly ascribed to the pinning effect of SiC particles by inhibiting the plastic deformation and fracture of softer matrix, and to the lubricating effect of oxide debris [22]. Similar behavior was confirmed for Al_2O_3-reinforced Ti_3SiC_2 composites (10 and 20 vol% Al_2O_3) against AISI-52100 steel balls tested in dry air in reciprocating mode. It was determined that the hard Al_2O_3 particles pin the surrounding soft matrix and delocalize the shear stresses, so, reducing the wear rate [23].

The previous reports were exclusively focused on isotropic MAX phases. However, because of their layered nature, it is expected that their wear behavior is strongly dependent on the crystallographic orientation. Recently, Hu *et al*. [24–27] fabricated the *c*-axis textured Nb_4AlC_3, Ti_3SiC_2, and Ti_3AlC_2 using the strong magnetic field alignment (SMFA) method followed by spark plasma sintering, and the resulting materials showed a shell-like mechanical behavior. These textured ceramics possessed marked anisotropic physical properties and outstanding mechanical response. For example, the tailored Nb_4AlC_3 ceramic showed the high flexural strength above 1200 MPa and high fracture toughness above 18 MPa·m$^{1/2}$ parallel to the *c*-axis direction [28]. The latter suggests that textured MAX phases might exhibit excellent wear resistance.

In the present work, the mean coefficient of friction and wear rate of textured Ti_3AlC_2 ceramic are investigated by characterizing the different texture directions against SUS304 balls at room temperature. The worn mechanisms on the different texture surfaces will be discussed.

2 Experimental procedure

The textured Ti_3AlC_2 ceramic was fabricated by strong magnetic field alignment method followed by spark plasma sintering as detailed in Ref. [27]. The density of textured Ti_3AlC_2 was 4.21 g/cm^3. The measured Vickers hardness on the TTS (7.4 GPa) was about 28% higher than that on the TSS (5.8 GPa). Samples for wear testing were machined by electrical discharge cutting. The samples with a dimension of 2 mm × 4 mm × 10 mm were employed; for each of them the 4 mm × 10 mm side was polished down to 0.5 μm diamond grids, resulting in a surface roughness of 20 nm. Figure 1 presents the schematic relationship between sliding direction of balls and texture surface of tailored Ti_3AlC_2. According to the anisotropic microstructure of textured Ti_3AlC_2 ceramic, the tested planes were named as textured top surface (TTS) and textured side surface (TSS-1 and TSS-2), as shown in Figs. 1(a)–1(c), respectively.

The reciprocating tribological testing was conducted by using an HEIDON facility (SHINTO Scientific Co.,

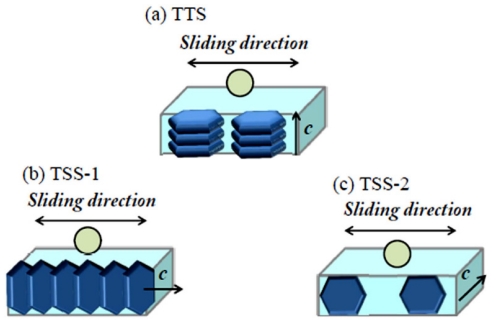

Fig. 1 Schematic figures of wear test along the different texture directions: (a) on the textured top surface (TTS), (b) on the textured side surface (parallel to *c* axis) (TSS-1), and (c) on the textured side surface (perpendicular to *c* axis) (TSS-2).

Ltd., Tokyo, Japan) with 500 times of cycling. The sliding distance of counterpair SUS304 balls with a diameter of 3 mm was 7 mm and the sliding speed was 1 mm/s. The load was set as 1, 5, and 9 N and the load error was below 10 g. For each load, three samples were tested along one direction (in total 27 samples were tested). The coefficient of friction was recorded in real time during the test. After testing, the collected wear debris and worn surface of samples and balls were examined by a JEOL5600 scanning electron microscope (SEM; JEOL Ltd., Tokyo, Japan) equipped with energy dispersive X-ray spectroscopy (EDS). After ultrasonic cleaning in ethanol for 30 min and drying in air, the worn samples were weighed by an electrical balance with a high accuracy of 0.1 mg. The wear volumes of samples were calculated based on the weight loss and density. And those of balls were calculated according to the diameter of worn surface using the spherical volume formula. Then the wear rates were calculated by an equation:

$$W = \frac{M}{LD} \tag{1}$$

in which M is the wear volume, L is the force, and D is the sliding distance [23]. In order to determine the worn mechanisms of anisotropic Ti_3AlC_2 ceramic, the ultrasonic cleaned worn surfaces were observed by SEM. Furthermore, Vickers indentions (50 N) on the worn surfaces were used to characterize the anisotropic wear damage of textured Ti_3AlC_2.

3 Results and discussion

3. 1 Texture microstructure of tailored Ti_3AlC_2

Figure 2 shows the X-ray diffraction (XRD) patterns

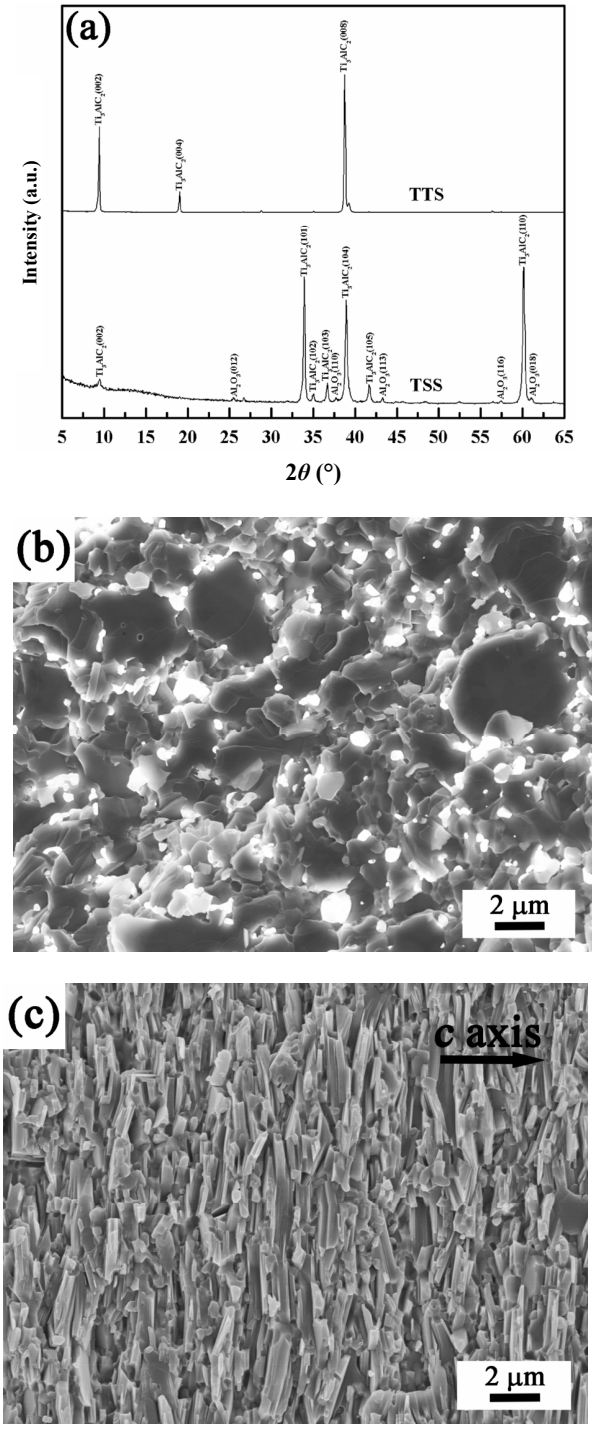

Fig. 2 (a) XRD patterns of textured top surface (TTS) and textured side surface (TSS) of tailored Ti_3AlC_2 ceramic, and SEM micrographs of fracture surfaces of (b) TTS and (c) TSS.

and texture microstructure of tailored Ti_3AlC_2 ceramic. It is observed that on the textured top surface (TTS), the typical diffraction peaks are (000*l*) basal plane. On the textured side surface (TSS), (101), (104), and (110) planes are corresponded to [11–20] axis direction (Fig.

2(a)). Additionally, the fracture surfaces of TTS and TSS exhibit that plate grains stack orderly (Figs. 2(b) and 2(c)), indicating the anisotropic shell-like microstructure. Also, it is observed that Al_2O_3 particles (about 15.4 vol%) homogeneously distribute in the Ti_3AlC_2 matrix, which might enhance the wear resistance of soft Ti_3AlC_2 matrix [27].

3. 2 Tribological behaviors

Table 1 lists the mean coefficient of friction of textured Ti_3AlC_2 as a function of load against SUS304 balls along different texture directions. The mean coefficient of friction was averaged for the whole time duration of the test and for the three samples tested for each orientation. The samples were tested under the loads of 1, 5, and 9 N. It is seen that the mean coefficient of friction increases in the order of TTS, TSS-1, and TSS-2 under the same load. On the TTS, the mean coefficient of friction shows a significant increase from 0.184 to 0.228 with the increment of load. The weak bondings on the basal planes between the Ti–C layers were fractured by the sliding balls on the contact surface of TTS sample [3]. Under higher load, more surface material on the contact region was scratched and removed by shearing mechanism. As a result, the sliding resistance became larger, resulting in higher mean coefficient of friction.

On the TSS-1, by increasing the load, the mean coefficient of friction increases from 0.245 to 0.250 and then decreases to 0.237. On the TSS-2, the mean coefficient of friction is achieved with the values of 0.257 (1 N), 0.289 (5 N), and 0.282 (9 N). It is suspected that on the TSS-1 and TSS-2, the scratch resistance undoubtedly shows the positive effect on the enhancement of coefficient of friction under the loads of 1 and 5 N. However, the reverse tendency of decrease of mean coefficient of friction under the load of 9 N is possibly ascribed to the formation of oxide debris which lubricated the countercouples so as to weaken the sliding resistance [29].

Tables 2 and 3 list the wear rates of textured Ti_3AlC_2 samples and SUS304 balls as a function of load, respectively. It is clearly seen that the wear loss of

Table 1 Mean coefficient of friction of tailored Ti_3AlC_2 ceramic against SUS304 balls along different texture directions

	1 N	5 N	9 N
TTS	0.184±0.007	0.219±0.004	0.228±0.016
TSS-1	0.245±0.019	0.250±0.003	0.237±0.014
TSS-2	0.257±0.005	0.289±0.005	0.282±0.001

Table 2 Wear rate of textured Ti_3AlC_2 ceramic tested along different directions under different loads

(Unit: 10^{-3}mm^3/(N·m))

	1 N	5 N	9 N
TTS	6.79±0.62	2.49±1.96	85.01±18.32
TSS-1	13.58±4.75	3.62±2.07	3.02±0.85
TSS-2	9.05±3.91	4.07±1.36	1.51±0.76

Table 3 Wear rate of corresponding SUS304 balls tested along different directions under different loads

(Unit: 10^{-5}mm^3/(N·m))

	1 N	5 N	9 N
TTS	12.67±2.49	30.78±3.12	272.56±46.13
TSS-1	2.97±0.17	7.16±1.95	15.81±1.54
TSS-2	3.13±1.14	1.51±0.20	1.77±0.24

textured Ti_3AlC_2 exhibits different values along different sliding directions under the same load, as shown in Table 2. On the TTS, the wear rate is as low as 6.79×10^{-3} mm^3/(N·m) under the load of 1 N. Under the same load, the wear rates on the TSS-1 and TSS-2 are 13.58×10^{-3} and 9.05×10^{-3} mm^3/(N·m), respectively. This suggests that the self-lubricant mechanism of Ti_3AlC_2 is comparable to the one occurring in graphite [30,31]. Therefore, considering the preferential nanolaminar microstructure of Ti_3AlC_2 grains, the lowest wear rate on the TTS is possibly ascribed to its self-lubricating behavior. When increasing the loads up to 5 and 9 N, the wear rate on the TTS exhibits an initial decrease to 2.49×10^{-3} mm^3/(N·m) and then increases greatly to 85.01×10^{-3} mm^3/(N·m). It is suggested that under the load of 5 N self-lubricity still contributes positively to wear rate. However, under the load of 9 N the material is prone to be removed quickly due to the weak bonding of basal planes.

Interestingly, for the specimens of TSS-1 and TSS-2, the wear rates show a continuous decrease with increasing load. For TSS-1 sample, the wear rates are 3.62×10^{-3} and 3.02×10^{-3} mm^3/(N·m) respectively under the loads of 5 and 9 N. And for TSS-2, those are 4.07×10^{-3} and 1.51×10^{-3} mm^3/(N·m) respectively. The reason for this is the existence of oxide debris on the wear tracks, such as Ti–O, Al–O, Fe–O, or Cr–O particles [32]. Even if the third body abrasion occurred during the testing, these oxide debris probably plays an important role on lubricating the counterpairs to weaken the scratching effect. Additionally, Barsoum *et al*. [33] found that Ti_3SiC_2 ceramic shows a fully strain reversible deformation when being compressed up to 1 GPa; after removing the load, 25% of the mechanical energy is dissipated. Such dissipation is attributed to the reversible formation and annihilation of incipient

kink bands when deforming at room temperature. Similarly, Jones *et al*. [34] investigated the reversible hysteresis of single Ti_3SiC_2 crystal by nano indentation and confirmed that it is associated with conventional dislocation flow. Owing to the similar crystal structure of Ti_3AlC_2, especially the grains' basal planes of TSS-2 sample are parallel to the sliding direction of balls, the shear stresses induce the dislocation walls along the basal planes and after unloading the dislocation walls disappear following the reversible elastic deformation. Therefore, the wear rate of TSS-2 sample could be effectively decreased based on the elastic recovery and energy dissipative mechanism inside the material.

In Table 3, the wear rates of SUS304 balls are given for the different surface orientations. The wear rates of balls increase from 12.67×10^{-5} to 272.56×10^{-5} $mm^3/(N\cdot m)$ with increasing loads of 1, 5, and 9 N for TTS samples. Similarly, those of balls counter-facing TSS-1 samples show a continuous increase from 2.97×10^{-5} to 15.81×10^{-5} $mm^3/(N\cdot m)$. This is ascribed to the larger contact surface area and the higher quantity of debris formed which increase the third body abrasion. However, the wear rates of SUS304 balls against TSS-2 samples show a reverse tendency, decreasing from 3.13×10^{-5} to 1.51×10^{-5} $mm^3/(N\cdot m)$ and then 1.77×10^{-5} $mm^3/(N\cdot m)$ with increasing load. This result might be associated with the less debris on the worn surface of TSS-2 samples with the increment of load, confirmed by Fig. 3.

3. 3 Worn mechanisms

Figure 3 shows the worn surface of textured Ti_3AlC_2 under the loads of 1 and 9 N along the different texture directions. The correspondent worn surfaces of SUS304 balls were also observed, as shown in Fig. 4. It is seen that under the load of 1 N on the worn surface of TTS sample some plates are kept to support the sliding balls, effectively enhancing the wear resistance (Fig. 3(a)). Some debris forms and deposits in pits. However, under the load of 9 N, the damage becomes extensive and only debris could be found on the wear track (Fig. 3(b)), which indicates that the basal planes have been easily debonded by shearing. That is why the wear rate of TTS sample is so high under 9 N, as indicated in Table 2. Similarly, the counter sliding balls present a clear shear wear induced damage by the third body under 9 N (Fig. 4(b)), which is more intense in comparison with the balls tested under 1 N (Fig. 4(a)).

On the worn surface of TSS-1 sample, though the spalling-off of grains caused by the shear stresses becomes more severe for 9 N than for 1 N and there are a plenty of debris filling in the pit regions (Figs. 3(c) and 3(d)), the protuberant plates could still

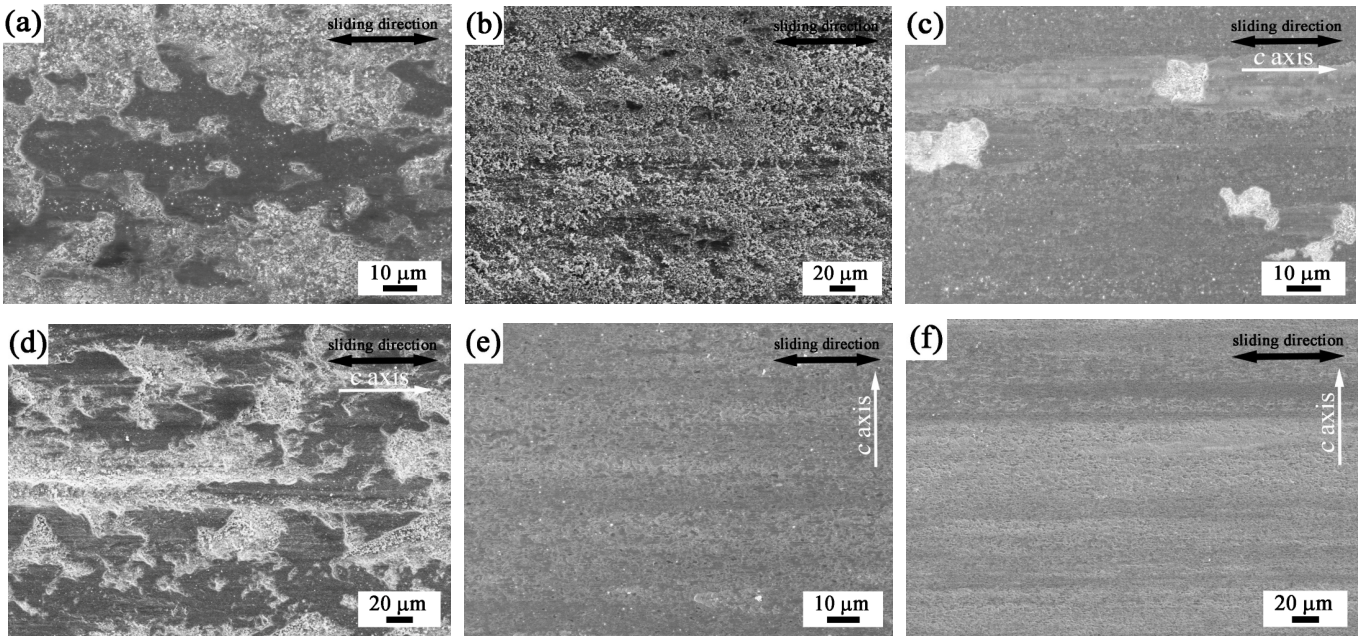

Fig. 3 SEM micrographs of worn surface of tailored Ti_3AlC_2 ceramic under the loads of 1 and 9 N along the different texture directions: (a, b) TTS sample, (c, d) TSS-1 sample, and (e, f) TSS-2 sample.

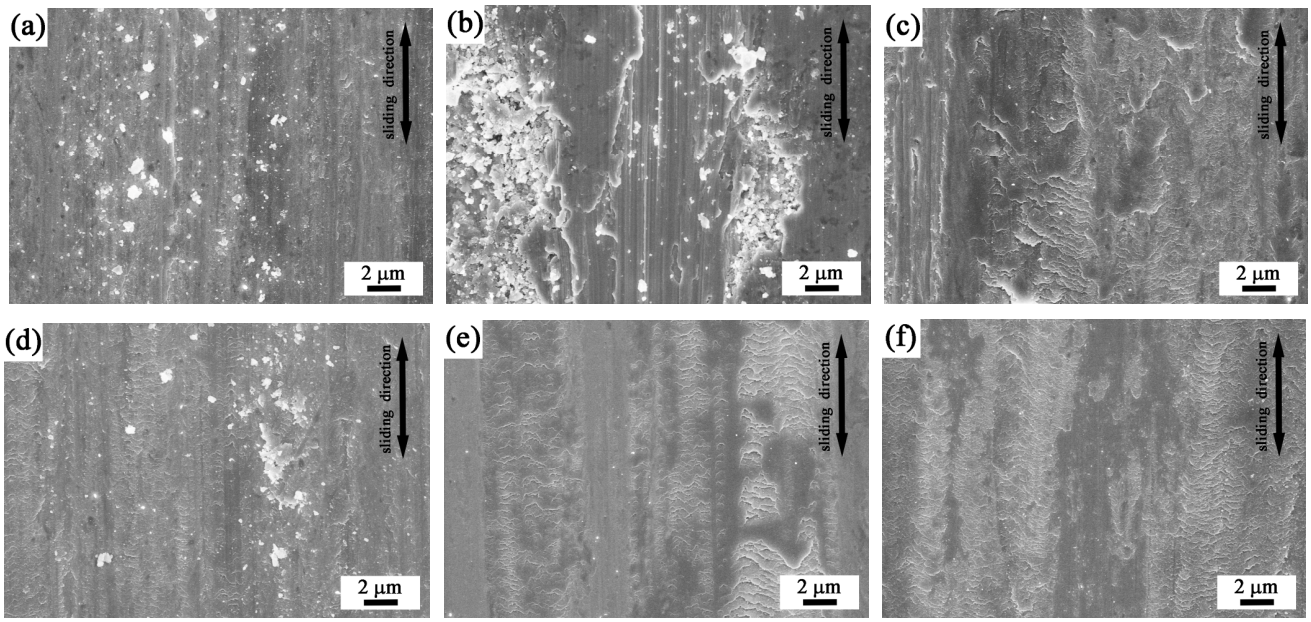

Fig. 4 SEM micrographs of worn surface of SUS304 balls tested under the loads of 1 and 9 N: (a, b) against TTS sample, (c, d) against TSS-1 sample, and (e, f) against TSS-2 sample.

effectively endure the rubbing of balls. So, the wear rate of TSS-1 sample shows an inverse tendency with increasing load. Reversely, the wear rates of counterpair balls increase with the increment of load owing to the worse third body abrasion, as shown in Figs. 4(c) and 4(d). When tested at 1 N, no debris can be found on the worn surface of balls and a layer of compacted debris is formed. Under the load of 9 N, the loose debris adheres onto the worn surface of balls, accelerating the wear loss of balls. Interestingly, on the worn surface of TSS-2 sample (Figs. 3(e) and 3(f)), even under the highest load of 9 N, there are no formed spalling-off regions and only tiny debris can be observed. It is why the wear rate of TSS-2 sample presents the decreasing value with increasing load. Similarly, on the worn surface of SUS304 balls (Figs. 4(e) and 4(f)), only compacted fish-scaled debris can be observed along the sliding direction. Due to the lack of the third body, the wear rates of balls also show the general decreasing tendency (Table 3).

Figure 5 shows the SEM micrographs of debris collected on the worn surface of Ti_3AlC_2 samples tested along different texture directions, as well as their EDS results. It is clearly seen that the debris consists of nano sized particles (Figs. 5(a)–5(c)), which means that the reciprocating wear process has effectively crushed the surface grains. The debris serves as the third body to strengthen the wear effect. In addition, it is detected that Ti, Al, Cr, Fe, C, and O elements exist in the debris. Wu *et al*. [35] have determined that the

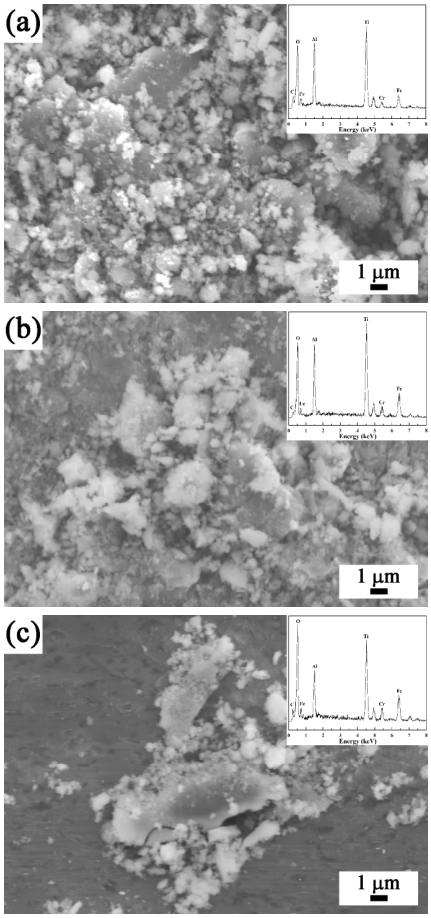

Fig. 5 SEM micrographs and EDS analysis of debris on the worn surface of tailored Ti_3AlC_2 ceramic tested under the load of 5 N: (a) TTS sample, (b) TSS-1 sample, and (c) TSS-2 sample.

dry sliding process in air could induce the oxidation of debris under the contact region of countercouples of Ti_3AlC_2/AISI-52100 bearing steel [35]. Possibly, TiO_2, Al_2O_3, and Fe_2O_3, etc., have been formed during the sliding, which contribute to lowering the coefficient of friction [36].

Figure 6 indicates the high magnification images of worn regions of tailored Ti_3AlC_2 after ultrasonic cleaning. On the TTS, the material remove mechanisms are determined as grains' delamination and peeling-off at the positions of basal planes (Fig. 6(a)). The sliding balls have scratched the texture grains layer by layer. For TSS-1 sample, the damage mechanisms are represented by the delamination and pulling-out of grains by scratching (Fig. 6(b)). Interestingly, for TSS-2 sample, only plowing tracks can be observed and no crushed grains are found on the worn surface (Fig. 6(c)).

In order to understand the mechanical responses of texture microstructure of textured Ti_3AlC_2 and to explain the worn mechanisms, the Vickers indents (load of 50 N) on the worn surface were examined as shown in Fig. 7. Clearly, it is seen that the morphologies of indents are different depending on the textured surface. On the TTS, the indent is a square (symmetric) and the materials are pushed out around the indented area by the shear stresses (Fig. 7(a)), indicating the isotropic (on the TTS plane) mechanical response. However, on the worn surface of TSS-1 sample, the indent shows rhombohedral shape (asymmetrical), reflecting its anisotropic mechanical response. Along the sliding direction of balls, the materials are easy to be delaminated, crushed, and pushed out, exhibiting the irreversible plastic deformation (Fig. 7(b)). Reversely, on the worn surface of TSS-2 sample, the rhombus indent shows that no crushed grains exist at the corners along the sliding direction and the diagonal line is shorter, proving the elastic recovery after the release of stresses (Fig. 7(c)). It is confirmed that the soft–hard combination with typical nanolaminar structure contributes to the excellent elastic mechanical

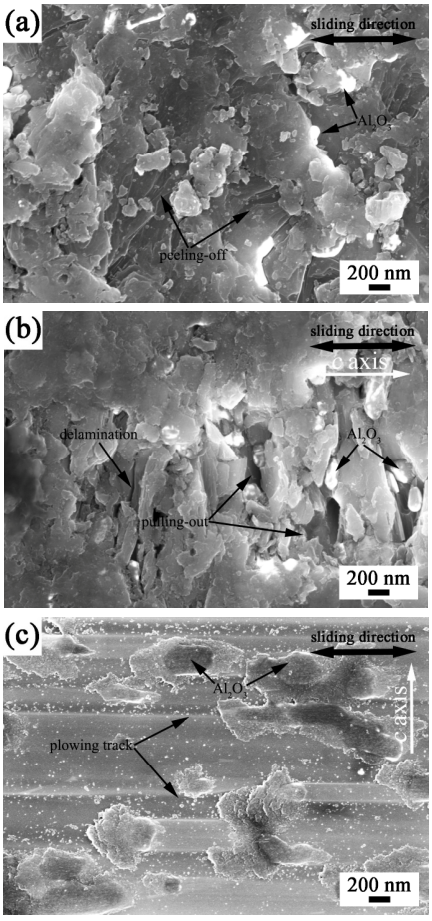

Fig. 6 Wear damages on different texture surfaces of tailored Ti_3AlC_2 ceramic when tested at 1 N: (a) TTS, (b) TSS-1, and (c) TSS-2.

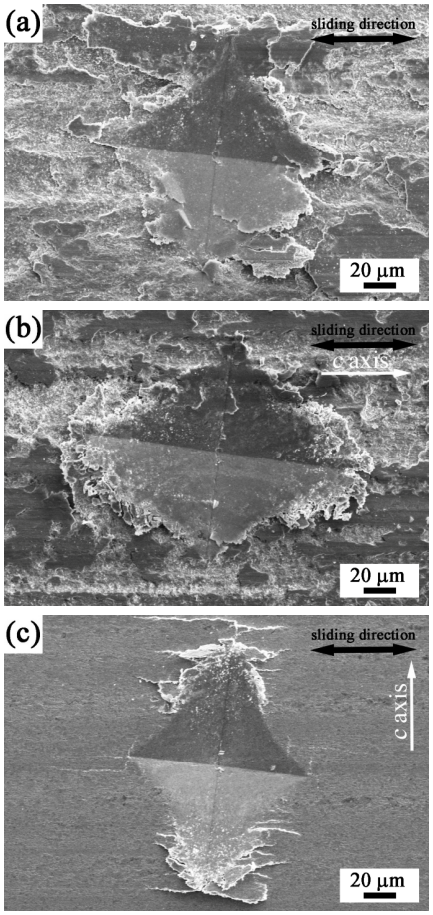

Fig. 7 Vickers indents induced by a load of 50 N on the worn surface of tailored Ti_3AlC_2 ceramic tested under 5 N: (a) TTS sample, (b) TSS-1 sample, and (c) TSS-2 sample.

reversibility. These experimental results strongly support that the preferential texture microstructure in Ti_3AlC_2 strongly affects its wear resistance.

4 Conclusions

Tribological behaviors of tailored Ti_3AlC_2 ceramic were investigated by using the reciprocating mode against SUS304 balls under the loads of 1, 5, and 9 N. The tribological properties (mean coefficient of friction and wear rate) were strongly affected by the crystallographic texturing. On the TTS ((000*l*) plane), the mean coefficient of friction showed the lowest value compared to those of TSS-1 and TSS-2 samples under the same load. On the TSS-2, the lowest wear rate of 1.51×10^{-3} $mm^3/(N\cdot m)$ was achieved when tested under the load of 9 N, and interestingly the wear rate showed a decreased value with the increased load. The worn mechanisms on the TTS and TSS-1 were confirmed as delamination, grain crushing, and grain pulling-out, and that of TSS-2 sample was mainly attributed to the plowing effect by scratching.

Acknowledgements

This work is supported by "ChuYing" Program of Southwest Jiaotong University and Thousand Talents Program of Sichuan Province. Also, we thank for the supports of National Natural Science Foundation of China (Nos. U1232136 and 91226202), Grant-in-Aid for Scientific Research B (No. 23350104) from Japan Society for the Promotion Science, the Fundamental Research Program of Korean Institute of Materials Science (KIMS), and UK EPSRC Material Systems for Extreme Environments Programme Grant (EP/K008749/1, XMat).

References

[1] Barsoum M, El-Raghy T. The MAX phases: Unique new carbide and nitride materials. *Am Sci* 2001, **89**: 334–343.
[2] Barsoum M, Radovic M. Mechanical properties of the MAX phases. *Encyclopedia Mater: Sci Tech* 2004: 1–16.
[3] Wang XH, Zhou YC. Layered machinable and electrically conductive Ti_2AlC and Ti_3AlC_2 ceramics: A review. *J Mater Sci Technol* 2010, **26**: 385–416.
[4] Sun ZM. Progress in research and development on MAX phases: A family of layered ternary compounds. *Int Mater Rev* 2011, **56**: 143–166.
[5] Eklund P, Beckers M, Jansson U, *et al*. The $M_{n+1}AX_n$ phases: Materials science and thin-film processing. *Thin Solid Films* 2010, **518**: 1851–1878.
[6] Zhang J, Liu B, Wang JY, *et al*. Low-temperature instability of Ti_2SnC: A combined transmission electron microscopy, differential scanning calorimetry, and X-ray diffraction investigations. *J Mater Res* 2009, **24**: 39–49.
[7] Lin Z, Zhuo M, Zhou Y, *et al*. Microstructure and theoretical bulk modulus of layered ternary tantalum aluminum carbides. *J Am Ceram Soc* 2006, **89**: 3765–3769.
[8] Zheng L, Wang J, Lu X, *et al*. $(Ti_{0.5}Nb_{0.5})_5AlC_4$: A new-layered compound belonging to MAX phases. *J Am Ceram Soc* 2010, **93**: 3068–3071.
[9] Hu C, Lai C-C, Tao Q, *et al*. Mo_2Ga_2C: A new ternary nanolaminated carbide. *Chem Commun* 2015, **51**: 6560–6563.
[10] Wan D, Zhou Y, Hu C, *et al*. Improved strength-impairing contact damage resistance of $Ti_3Si(Al)C_2$/SiC composites. *J Eur Ceram Soc* 2007, **27**: 2069–2076.
[11] Lee DB, Park SW. High-temperature oxidation of Ti_3AlC_2 between 1173 and 1473 K in air. *Mat Sci Eng A* 2006, **434**: 147–154.
[12] Zhu J, Ye L, He L. Microstructure and mechanical properties of in situ synthesized Ti_2AlC/Al_2O_3 composites. *Mat Sci Eng A* 2012, **547**: 6–11.
[13] Duan X, Shen L, Jia D, *et al*. Synthesis of high-purity, isotropic or textured Cr_2AlC bulk ceramics by spark plasma sintering of pressure-less sintered powders. *J Eur Ceram Soc* 2015, **35**: 1393–1400.
[14] Heinzel A, Müller G, Weisenburger A. Compatibility of Ti_3SiC_2 with liquid Pb and PbBi containing oxygen. *J Nucl Mater* 2009, **392**: 255–258.
[15] Tallman DJ, Hoffman EN, Caspi EN, *et al*. Effect of neutron irradiation on select MAX phases. *Acta Mater* 2015, **85**: 132–143.
[16] Nappé JC, Monnet I, Grosseau P, *et al*. Structural changes induced by heavy ion irradiation in titanium silicon carbide. *J Nucl Mater* 2011, **409**: 53–61.
[17] Gupta S, Filimonov D, Zaitsev V, *et al*. Ambient and 550 ℃ tribological behavior of select MAX phases against Ni-based superalloys. *Wear* 2008, **264**: 270–278.
[18] Gupta S, Filimonov D, Palanisamy T, *et al*. Tribological behavior of select MAX phases against Al_2O_3 at elevated temperatures. *Wear* 2008, **265**: 560–565.
[19] Ren S, Lu J, Jia Q, *et al*. Tribochemistry of Ti_3SiC_2/Si_3N_4 tribopair in ethanol. *Tribol Int* 2014, **74**: 174–180.
[20] Ren S, Meng J, Wang J, *et al*. Tribo-corrosion behaviors of Ti_3SiC_2/Si_3N_4 tribo-pair in hydrochloric acid and sodium hydroxide solutions. *Wear* 2012, **274–275**: 8–14.
[21] Zhu Y, Zhou A, Ji Y, *et al*. Tribological properties of Ti_3SiC_2 coupled with different counterfaces. *Ceram Int* 2015, **41**: 6950–6955.
[22] Wan DT, Hu CF, Bao YW, *et al*. Effect of SiC particles on the friction and wear behavior of $Ti_3Si(Al)C_2$-based composites. *Wear* 2007, **262**: 826–832.
[23] Hu C, Zhou Y, Bao Y, *et al*. Tribological properties of polycrystalline Ti_3SiC_2 and Al_2O_3-reinforced Ti_3SiC_2 composites. *J Am Ceram Soc* 2006, **89**: 3456–3461.

[24] Hu C, Sakka Y, Tanaka H, *et al*. Fabrication of textured Nb_4AlC_3 ceramic by slip casting in a strong magnetic field and spark plasma sintering. *J Am Ceram Soc* 2011, **94**: 410–415.

[25] Hu C, Sakka Y, Nishimura T, *et al*. Physical and mechanical properties of highly textured polycrystalline Nb_4AlC_3 ceramic. *Sci Technol Adv Mat* 2011, **12**: 44603–44608.

[26] Hu C, Sakka Y, Grasso S, *et al*. Tailoring Ti_3SiC_2 ceramic via a strong magnetic field alignment method followed by spark plasma sintering. *J Am Ceram Soc* 2011, **94**: 742–748.

[27] Zhang HB, Hu CF, Sato K, *et al*. Tailoring Ti_3AlC_2 ceramic with high anisotropic physical and mechanical properties. *J Eur Ceram Soc* 2015, **35**: 393–397.

[28] Hu C, Sakka Y, Grasso S, *et al*. Shell-like nanolayered Nb4AlC3 ceramic with high strength and toughness. *Scripta Mater* 2011, **64**: 765–768.

[29] Huang Z, Zhai H, Guan M, *et al*. Oxide-film-dependent tribological behaviors of Ti_3SiC_2. *Wear* 2007, **262**: 1079–1085.

[30] Ma J, Hao J, Fu L, *et al*. Intrinsic self-lubricity of layered Ti_3AlC_2 under certain vacuum environment. *Wear* 2013, **297**: 824–828.

[31] Zhou AG, Barsoum MW, Basu S, *et al*. Incipient and regular kink bands in fully dense and 10 vol.% porous Ti_2AlC. *Acta Mater* 2006, **54**: 1631–1639.

[32] Gupta S, Barsoum MW. On the tribology of the MAX phases and their composites during dry sliding: A review. *Wear* 2011, **271**: 1878–1894.

[33] Barsoum MW, Zhen T, Kalidindi SR, *et al*. Fully reversible, dislocation-based compressive deformation of Ti_3SiC_2 to 1 GPa. *Nat Mater* 2003, **2**: 107–111.

[34] Jones NG, Humphrey C, Connor LD, *et al*. On the relevance of kinking to reversible hysteresis in MAX phases. *Acta Mater* 2014, **69**: 149–161.

[35] Wu L, Chen J, Liu M, *et al*. Reciprocating friction and wear behavior of Ti_3AlC_2 and Ti_3AlC_2/Al_2O_3 composites against AISI52100 bearing steel. *Wear* 2009, **266**: 158–166.

[36] Lindquist M, Wilhelmsson O, Jansson U, *et al*. Tribofilm formation from TiC and nanocomposite TiAlC coatings, studied with focused ion beam and transmission electron microscopy. *Wear* 2009, **266**: 988–994.